Supporting Information

Branched Aramid Nanofibers

Jian Zhu, Ming Yang, Ahmet Emre, Joong Hwan Bahng, Lizhi Xu, Jihyeon Yeom, Bongjun Yeom, Yoonseob Kim, Kyle Johnson, Peter Green, and Nicholas A. Kotov*

ange_201703766_sm_miscellaneous_information.pdf
ange_201703766_sm_video_S1.mp4
ange_201703766_sm_video_S2.wmv
ange_201703766_sm_video_S3.wmv

Contents:

Section S1. Materials and Methods

    S1.1. Preparation of BANF dispersions
    S1.2. Preparation of cylindrical BANF hydrogels
    S1.3. Preparation of BANF continuous hydrogel fibers
    S1.4. Preparation of BANF hydrogel sheets
    S1.5. Preparation of PVA/BANF composites
    S1.6. Porosity Estimation in the aerogels
    S1.7. Other Characterization tools

Section S2. Additional notes about mechanical properties of BANF 3DNs

Section S3. Additional notes mechanical properties of BANF-PVA composites.

Section S4. Supporting Figures

    Figure S1. AFM analyses of BANFs.
    Figure S2. ANFs prepared using KOH and EtOK.
    Figure S3. Preparation of BANF hydrogels.
    Figure S4. Photoluminescence of BANF excited at 380 nm.
    Figure S5. BANF aerogels under compression.
    Figure S6. Fabrication of BANF/PVA composites.
    Figure S7. Mechanical and thermal properties BANF/PVA composites.

Section S1. Materials and Methods

1.1. Preparation of BANF dispersions

    1% branched aramid nanofiber (BANF) dispersion was prepared by stirring Kevlar 69 (from Thread Exchange, right twist) in dimethyl sulfoxide (DMSO) for one week in the presence of KOH (1 g/100 mL DMSO). This dispersion was used to prepare hydrogels and aerogels in this study. A comparative study substituted potassium ethoxide (EtOK) for KOH in the procedure to prepare the ANF dispersion.

1.2. Preparation of ANF cylindrical hydrogels

    4 mL of the as-prepared dispersion was put into a cylindrical tube, and 10 mL deionized (DI) water was slowly dropped on top of the ANF dispersion to minimize disturbance. Phase segregation started immediately and was completed within 12 hours to form an ANF hydrogel. Fresh DI water was added two times a day for four days to completely replace DMSO in the ANF hydrogel. The solid content of the BANF hydrogel was estimated by completely drying the hydrogel in a 100 °C oven overnight and measuring the weight difference. In order to prepare the BANF aerogels, water in the hydrogels was first exchanged with ethanol, and then dried using supercritical CO_2.

1.3. Preparation of ANF continuous hydrogel fibers

    0.1% BANF dispersion was extruded from a 28G stainless steel needle at a rate of 3 mL/h into a flow of DI water at a rate of 12 mL/h. The continuous gel fiber was immediately formed at the tip of the needle, and was guided into a 0.58 mm (ID) glass capillary tube, and then collected in a DI water reservoir. The flow rates were controlled by two syringe pumps, and soft silicone tubing was used for connection. A similar setup was used in an attempt to produce CellNF gel fibers by replacing DI water with acetone or isopropanol.

1.4. Preparation of BANF hydrogel sheets

The 1% BANF dispersion was confined between two pieces of 2" by 3" clean glass slides at a distance of ~0.2 mm, and was then immersed into DI water. The hydrogel sheet thickness was controlled by a spacer between the two glass slides (Figure S1a). Within 12 hours, the BANF hydrogel sheet was peeled off from the glass slides in water. The hydrogel sheet was then transferred into fresh water for storage.

1.5. Preparation of PVA/BANF composites

The ANF hydrogel sheet was immersed in 1 wt% PVA (Aldrich, Mowiol® 56-98, Mw ~195000) for 12 hours, and then rinsed with fresh water for 5 min. The thin sheet was then carefully transferred onto a piece of Teflon sheet and dried in a 70 °C oven for 30 min.

1.6. Porosity estimation in the aerogels

The porosity was estimated by the following equation:

$$Porosity = 1 - \frac{\rho_{gel}}{\rho_{solid}}$$

where ρ_{gel} and ρ_{solid} are the density of the aerogel and its constituent solid, respectively. The following densities were used to calculate aerogel porosity in this study: Kevlar (1.44 g/cm^3), cellulose (1.5 g/cm^3), carbon nanotubes (1.3 g/cm^3), graphene (2.26 g/cm^3), polyethylene glycol (1 g/cm^3), agarose (1.2 g/cm^3).

1.7. Other Characterization tools

The film transparency was determined by an 8453 UV-vis ChemStation spectrophotometer from Agilent Technologies. The cross-section and morphology of the film were examined using a FEI NOVA Nanolab scanning electron microscope (SEM) or JEOL 2100F S/TEM. Tapping mode

atomic force microscopy (AFM) images were obtained using a NanoScope IIIa atomic force microscope from Veeco Instruments. Transmission Electron Microscopy (TEM) was carried out using a JEOL 2100F instrument. 3D TEM tomography was performed on a Tecnai F20 electron microscope equipped a Gatan CCD camera and a field emission gun run at 200 keV. Gold nanoparticles of 15 nm in diameter were used as fiducial markers to aid tracking and alignment.

Differential scanning calorimetry (DSC) was carried out on a TA instrument Discovery DSC under nitrogen atmosphere at a temperature ramp rate of 20 °C/min. To eliminate thermal history, the samples went through steps of heating-cooling-heating according to the protocol in ASTM D3418–08. The second heating step was used for analysis. PVA content can then be estimated by comparing the PVA melt enthalpy in the composite with that in pure PVA. Thermogravimetric analysis (TGA) was run on a TA instrument Discovery TGA with a heating rate of 10 °C/min in nitrogen. The coefficient of thermal expansion (CTE) of films was measured using extension mode in Perkin Elmer TMA7, following ASTM *Test Method for Linear Thermal Expansion of Solid Materials by Thermomechanical Analysis* (E 831) and slightly modified to measure the thin film. The extension probe and grips were customized by RT instruments, Inc., to minimize the expansion of grips during the measurement. A ramp rate of 5 °C/min was used and the second heating step was used for analysis.

The viscosities of ANF dispersions were measured using an AR-G2 rheometer (TA instruments), using a 40 mm 2° cone and plate configuration. Measurements were performed at 25 °C. The rheological (shear) measurement for hydrogels was conducted on a TA Instruments' AERS rheometer with a 25 mm cone-plate geometry at 25 °C. Dynamic frequency sweep experiments were set from 0.06 to 60 rad/s at a fixed oscillatory strain of 1 %. The strain sweep experiments were set from 0.1% to 100% at a fixed frequency of 6 rad/s. The samples were covered

with a thin layer of silicon oil to prevent evaporation of water. Uniaxial tensile testing was done on a RSAIII Rheometrics Systems Analyzer from TA instruments. The tensile tests confirm to the ASTM standard ASTM D882. In a typical measurement, a 1 mm wide and 6 mm long sample strip was fixed onto the steel grips. The Kevlar microfiber was fixed by super-gluing the ends onto two pieces of stainless steel metal sheets separated by a distance of 6 mm. The metal sheets were then put between the grips for measurement. The test speed was 0.01 mm/s. A total of six measurements were made for two batches of PVA/ANF composite. A total of three measurements were made for the Kevlar microfiber.

Section S2. Additional notes about mechanical properties of ANF 3DNs

The ANF hydrogels and aerogels also exhibited satisfying performances in compression tests. The compressive strain-stress curves show three stages typical for porous materials (Figure 3e)[1]. The linear elastic stage was observed initially, then the material reached its elastic limit, at which point the 3DNs started to yield at a nearly constant stress. This plateau stage is followed by a densification region where the porous network starts to collapse. Both gels can be compressed to strains over 90% without any cracks at the macro-, micro-, or nanoscale (Figure S4 d, e, and f). Other 3DNs exhibit substantially higher brittleness. For example, graphene hydrogels show micro-cracks and stress discontinuity at a strain of ~45%[2], and cellulose aerogels become completely fractured at ~65% strain[3].

The compressive modulus E and yield stress σ_y for the ANF hydrogel are 57±3 kPa and 8±1 kPa. BANF aerogel has twofold higher values, E=90±5 kPa and σ_y=18±1 kPa. Note, however, that the plasticization effect of water on the ANF hydrogel is less pronounced than for other 3DNs. For example, highly porous (>99%) CellNF and CNT hydrogels are so compliant that they are

reminiscent of a viscous fluid.[3-5] Their 3D structure is disturbed by swelling in water and/or agitation. Instead, the BANF gels are stable in water for over a year without any visible fluidization. Even intensive sonication cannot destroy their structural integrity, while other un-crosslinked CNTs or CelluNFs do not survive the same treatment.

We also made a comparison of the compressive properties of BANF 3DNs to other commonly used reinforcing networks (Figure S4g) in the form of aerogels. The E of BANF aerogels is similar to that of CelluNF or CNT aerogels, but two orders of magnitude higher than graphene aerogels at a similar density. The similarity is likely due to the insufficient load transfer between the ligaments during the compression,[6] unlike the network deformation during the shearing. The nanofibers or nanotubes are likely to buckle or dislocate under stress due to their small diameters, as the bending modulus is of the order of $E_{fiber}d^4$, in which E_{fiber} and d are the elastic modulus and the diameter of the fiber[7], respectively. The graphene aerogel is especially prone to being bent due to its extreme thinness (~1 nm).

The tensile properties of BANF hydrogels and aerogels were studied further. The Young's modulus E_y, ultimate stress σ_u, and ultimate strain s_u of BANF hydrogels in tension are 230±18 kPa, 24±4 kPa, and 13±2%. The same parameters for ANF aerogels are E_y =750±10 kPa, σ_u=90±7 kPa, and s_u=12±3% (Figure 3f). The Young's modulus (E_y) of the BANF 3DNs in extension is much higher than that obtained in compression. Note that mechanical properties of BANF aerogels are typically higher than those of BANF hydrogels due to the absence of plasticization effect of water and the lack of hydrogen bonding competition between BANF and water. Due to the fluidity of CNT, CellNF, and graphene hydrogels at similar solid contents, their tensile properties are not available to compare. An indirect comparison with hydrogels with 1.2% CellNFs but reinforced with 30% PEG still shows that BANF hydrogels have higher Young's Moduli.[8] In addition, the

E_y of BANF hydrogels is 10 times higher than that of PEG hydrogels with much higher solid contents (Table S2).

From a practical perspective, it might be useful to increase tensile properties by sacrificing porosity. After an ANF aerogel is compacted into 1/6th of its initial volume, it displays E_y, s_u, and σ_u of 16±2 MPa, 11±2%, and 1.3±0.7 MPa, respectively. These properties can be further improved to 136±11MPa, 7±2%, and 6.2±0.5 MPa when the aerogel is further compressed (Figure 3f). Such enhancement is likely to originate from the increased density of hydrogen-bonding crosslinks and the nanofiber alignment in the film (Figure S4d, e, and f). The densified BANF 3DNs have ultimate stress comparable to σ_u of CNT buckypaper[9] but with seven times higher ultimate strain.

**Section S3. Additional notes on the mechanical properties of BANF-PVA composites.**

Drop casting or vacuum-assisted assembly is typically used for fabricating nanocomposites,[10,11] however, it is likely to induce nanofiller agglomeration or defect formation during these uncontrolled processes, which might lead to degraded mechanical properties. To overcome this challenge and attain reasonably high σ_u and s_u parameters, several bottom-up methods have been utilized. For example, laminated chitosan/alumina platelet composites[12] show σ_u values of 315±95 MPa and s_u values of 21±5%, and layer-by-layer assembled PVA and CNT composites[13] show σ_u values of 225±25 MPa and s_u values of 19±7%. However, these methods are generally time- and labor-intensive.

The inclusion of BANFs, which have a negative coefficient of thermal expansion (CTE) in the axial direction, greatly reduces the overall CTE of the composite.[14] Below the glass transition temperature (T_g), the PVA/BANF composite has a CTE of 1.9 ppm K^{-1}, which is smaller than a majority of ceramics, such as borosilicate glass (3.2-4.0 ppm K^{-1}), silicon (2.2-2.7 ppm K^{-1}) and
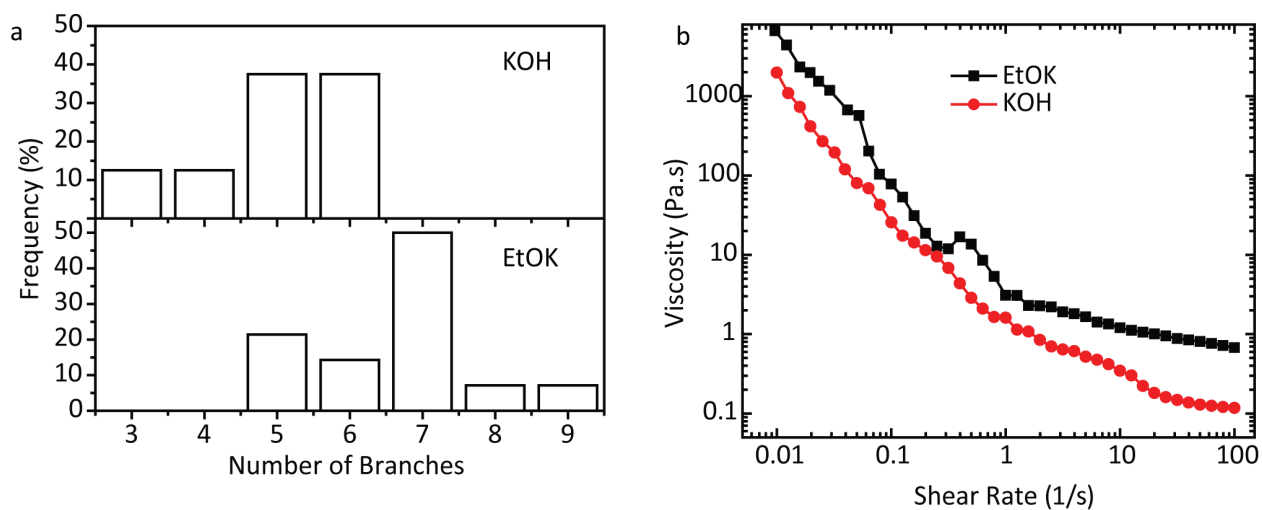
boron carbide (3.2-3.4 ppm K^{-1})[1]. Above T_g, the composite has a CTE of 32 ppm K^{-1}, close to that of neat PVA in the glassy state (Figure S7b).
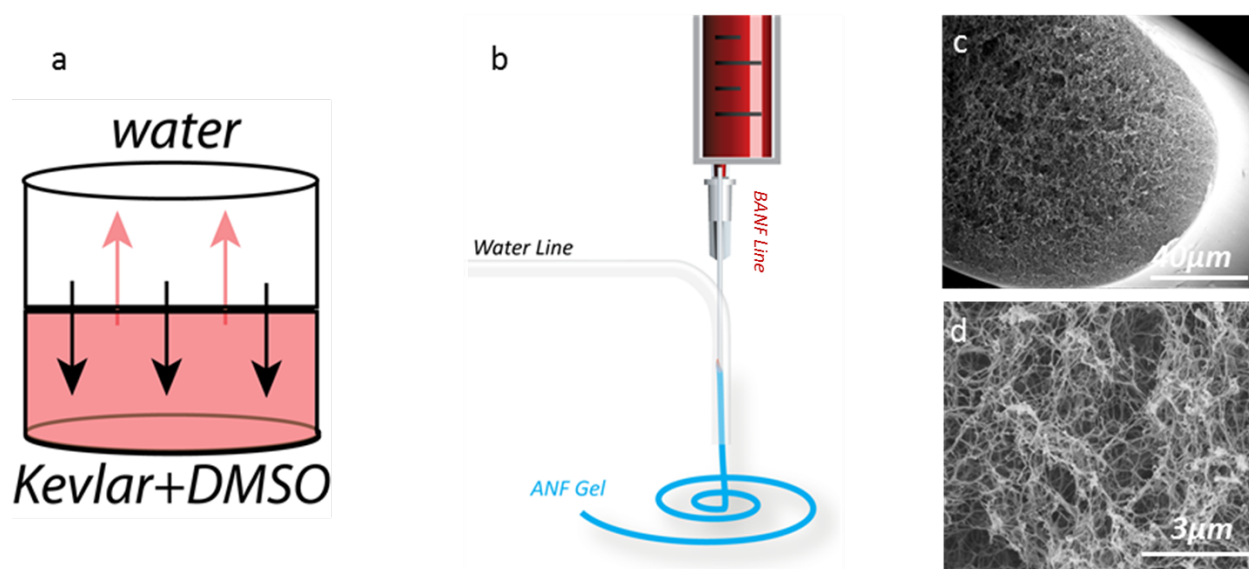
Section S4. Supporting Figures
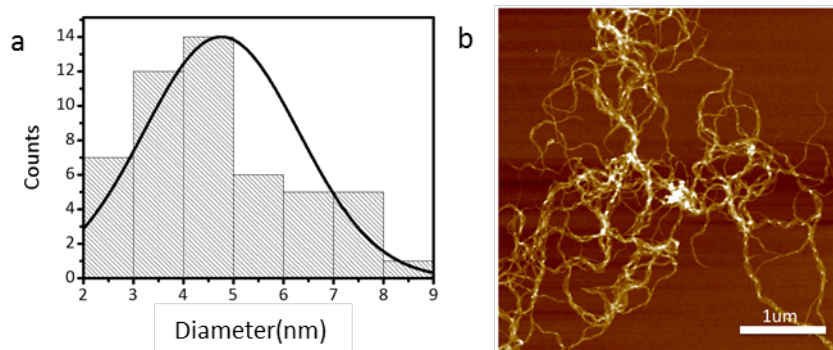
Figure S1. AFM analyses of BANFs. a) Statistical analysis of BANF diameters obtained from multiple AFM images. b) AFM image showing entangled BANFs.


Figure S2. BANFs prepared using KOH and EtOK. a) Histograms of number of branches on BANFs using KOH and EtOK. b) Viscosity of 1% BANF dispersion prepared using KOH and EtOK *vs.* shear rate.
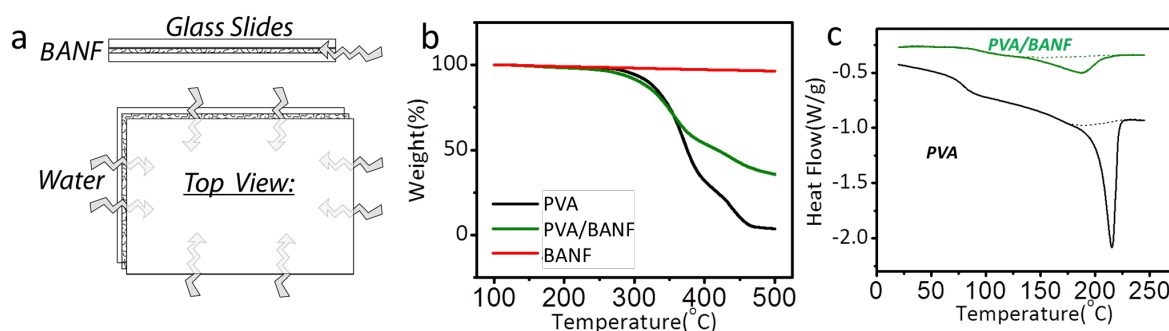
Figure S3. Preparation of BANF hydrogels. a) Schematic drawing of the solvent exchange process for BANF hydrogel. b) Schematic showing the BANF hydrogel-fiber production process. c) SEM image of the fibrous aerogel converted from hydrogel by supercritical CO_2 drying. d) Zoomed image showing internal BANF networks.
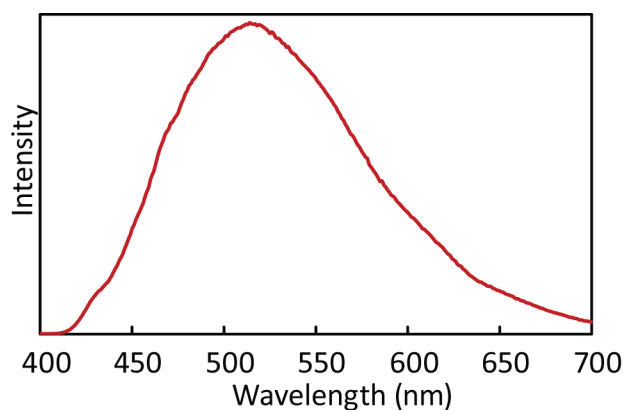

Figure S4. Photoluminescence of BANF excited at 380 nm.
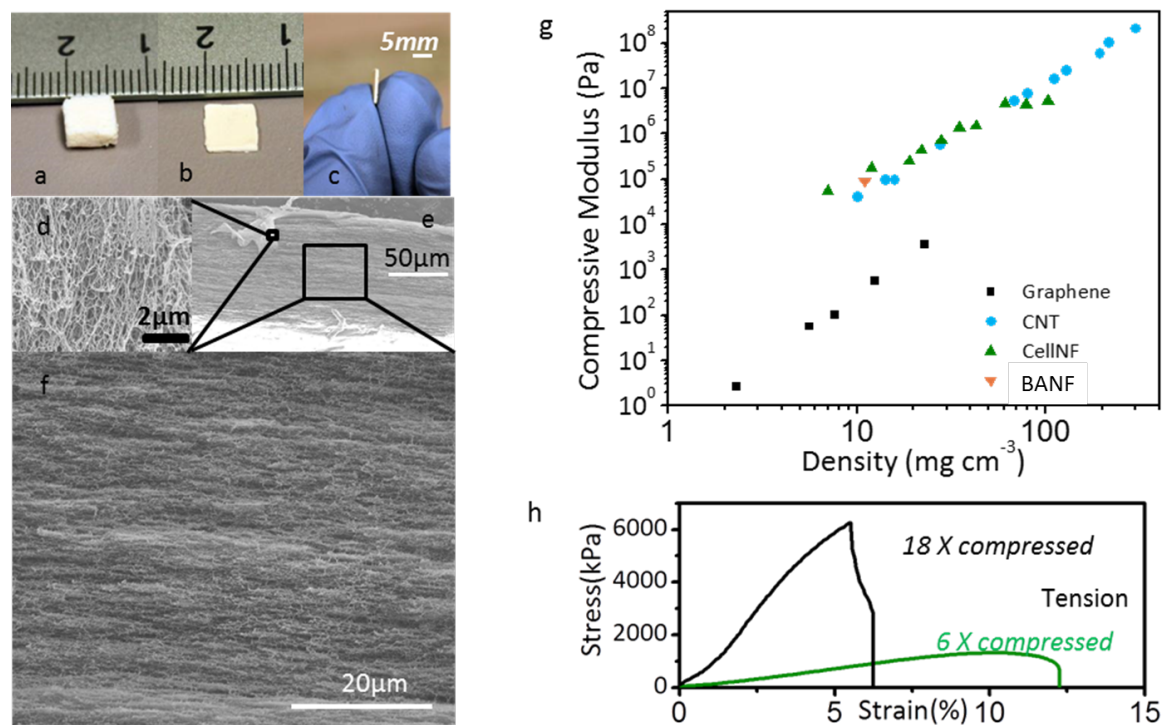
Figure S5. BANF aerogels under compression. a) BANF aerogel before compression. b) The same aerogel after compression. c) Side view photograph of the compressed aerogel. (d-f) SEM images of fractured edge in the compressed BANF aerogel at different magnifications. g) Compressive modulus *vs*. density of various aerogels in comparison to the BANF aerogels in this study. References: Graphene,[15] CNT, [16] CellNF.[17] h) Tensile stress-strain curves for BANF aerogel compressed into 1/6th and 1/18th of the initial height.

Figure S6. Fabrication of BANF/PVA composites. a) Schematic of the preparation of BANF hydrogel sheets. b) TGA of PVA, BANF and PVA/BANF composite. c) DSC analyses of PVA and the PVA/BANF composite.
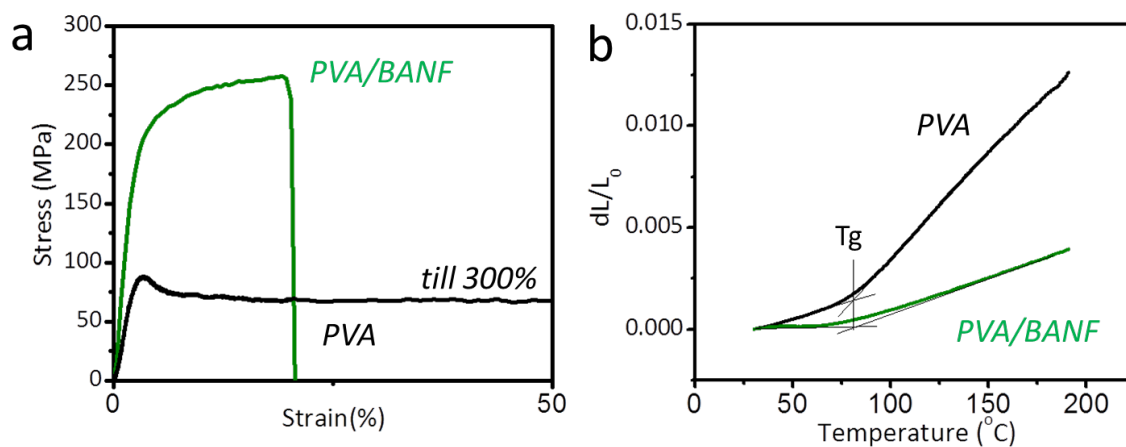
Figure S7. Mechanical and thermal properties BANF/PVA composites. a) Stress-strain curves for PVA and PVA/BANF films. b) Relative length change dL/L_0 for PVA and the PVA/BANF composite for a temperature scan from 30 °C to 190 °C. dL is the absolute length change while L_0 is the initial length at 30 °C.

Table S1 Comparison of storage moduli (*G'*) of various hydrogels in rheological studies. The highest value in G' column is highlighted in **red**.

Hydrogels	Crystalline Modulus(GPa)	Solid Content (wt%)	G'(kPa)
PLLA-PEO-PLLA triblock polymer[18]		18	10
Polyacrylamide[19]		5	0.2
carbon nanotube[20,21]	270-1470[22]	1	0.1
cellulose nanofiber[5,23,24]	111-220[25]	1	0.1-14
clay[26]		2	0.5
Clay/sodium polyarylate(SPA)[26]		2	4
BANF (this work)	153-182[27]	1	**29**
Graphene Oxide[28]	185-500[29,30]	1.6	0.05

Table S2 Comparison of mechanical properties of various hydrogels. The highest value in each column is highlighted in **red**.

		Compression		Tension		
	Solid Content (wt%)	Yield Strength (kPa)	Modulus (kPa)	Young's Modulus (kPa)	Strain (%)	Stress (kPa)
Graphene[2] Hydrogel	0.9	3	29	-	-	-
Cellulose Hydrogel[31]	10	-	7	2900	21	2200
Cellulose[8]	1.2%+30%PEG			26.1	970	325
Agarose Hydrogel[32]	2.25	-	28	-	-	-
PEG Hydrogel[32]	7.34	-	36	-	-	-
PEG Hydrogel[33]	25	-	-	23.1	53	12
BANF Hydrogel	1	8±1	57±3	230±18	13±2	24±4

Note that even hydrogels with 1.2% cellulose nanofiber and 30% PEG still have inferior Young's moduli in comparison to hydrogels with 1% BANF. PEG in this table stands for polyethylene glycol.

Table S3 Comparison of mechanical properties of various aerogels. The highest value in each column is highlighted with **red**.

	Porosity	Density (mg/cm3)	Relative Density#	Compression		Tension		
				Yield Strength (kPa)	Modulus (kPa)	Young's Modulus (kPa)	Strain (%)	Stress (kPa)
Graphene[15] Aerogel	99.4%	12.44	0.0055	-	0.556			
SWNT Aerogel[34,35]	99.4%	8.8	0.0067	20	100-120			
SWNT Aerogel[16]	99.2%	10	0.0077	-	40.5			
Cellulose Aerogel[3,5]	98.7%	20	0.0133	75	187.5			
Cellulose Aerogel[17]	99.5%	7	0.0047	7.8	56			
Cellulose Aerogel[17]	99.2%	12	0.0080	29.6	180			
BANF Aerogel	99.2%	11	0.0076	18±1	90±5	750±10	12±3	90±7
BANF Aerogel (6X)*	95.94%	66	0.0458			$(16\pm2)\times10^3$	11±2	$(1.3\pm0.7)\times10^3$
BANF Aerogel (18X)**	86.25%	198	0.1375			$(136\pm11)\times10^3$	7±2	$(6.2\pm0.5)\times10^3$

*,** 6X and 18X indicate that the volumes of BANF aerogels are compressed into 1/6th or 1/18th of their initial volumes.

#Relative density is defined as the density of aerogel divided by the density of single fiber.

REFERENCES:

[1]   M. F. Ashby, *Materials selection in mechanical design*, Elsevier, Maryland Heights 2005.

[2]   Y. X. Xu, K. X. Sheng, C. Li, G. Q. Shi, *Acs Nano* **2010**, *4*, 4324.

[3]   M. Paakko, J. Vapaavuori, R. Silvennoinen, H. Kosonen, M. Ankerfors, T. Lindstrom, L. A. Berglund, O. Ikkala, *Soft Matter* **2008**, *4*, 2492.

[4]   L. A. Hough, M. F. Islam, B. Hammouda, A. G. Yodh, P. A. Heiney, *Nano Lett* **2006**, *6*, 313.

[5]   M. Pääkkö, M. Ankerfors, H. Kosonen, A. Nykänen, S. Ahola, M. Österberg, J. Ruokolainen, J. Laine, P. T. Larsson, O. Ikkala, T. Lindström, *Biomacromolecules* **2007**, *8*, 1934.

[6]   L. R. Meza, S. Das, J. R. Greer, *Science* **2014**, *345*, 1322.

[7]   C. P. Broedersz, F. C. MacKintosh, *Rev Mod Phys* **2014**, *86*, 995.

[8]   J. Yang, C. R. Han, J. F. Duan, F. Xu, R. C. Sun, *Acs Appl Mater Inter* **2013**, *5*, 3199.

[9]   G. H. Xu, Q. Zhang, W. P. Zhou, J. Q. Huang, F. Wei, *Applied Physics A: Materials Science & Processing* **2008**, *92*, 531—539.

[10]   M. Nogi, S. Iwamoto, A. N. Nakagaito, H. Yano, *Advanced Materials* **2009**, *21*, 1595.

[11]   H. Sehaqui, Q. Zhou, L. A. Berglund, *Soft Matter* **2011**, *7*, 7342.

[12]   L. J. Bonderer, A. R. Studart, L. J. Gauckler, *Science* **2008**, *319*, 1069.

[13]   B. S. Shim, J. Zhu, E. Jan, K. Critchley, S. S. Ho, P. Podsiadlo, K. Sun, N. A. Kotov, *Acs Nano* **2009**, *3*, 1711.

[14]   J. Zhu, C. M. Andres, J. Xu, A. Ramamoorthy, T. Tsotsis, N. A. Kotov, *Acs Nano* **2012**, *6*, 8357.

[15]   H. Y. Sun, Z. Xu, C. Gao, *Advanced Materials* **2013**, *25*, 2554.

[16]   M. A. Worsley, S. O. Kucheyev, J. H. Satcher, A. V. Hamza, T. F. Baumann, *Applied Physics Letters* **2009**, *94*, 073115.

[17]   H. Sehaqui, M. Salajkova, Q. Zhou, L. A. Berglund, *Soft Matter* **2010**, *6*, 1824.

[18]   K. A. Aamer, H. Sardinha, S. R. Bhatia, G. N. Tew, *Biomaterials* **2004**, *25*, 1087.

[19]   C. Storm, J. J. Pastore, F. C. MacKintosh, T. C. Lubensky, P. A. Janmey, *Nature* **2005**, *435*, 191.

[20]   E. K. Hobbie, D. J. Fry, *J Chem Phys* **2007**, *126*.

[21]   Z. H. Fan, S. G. Advani, *J Rheol* **2007**, *51*, 585.

[22]   C. Lee, X. D. Wei, J. W. Kysar, J. Hone, *Science* **2008**, *321*, 385.

[23]   A. Mihranyan, K. Edsman, M. Strømme, *Food Hydrocolloids* **2007**, *21*, 267.

[24]   M. Chau, S. E. Sriskandha, D. Pichugin, H. Therien-Aubin, D. Nykypanchuk, G. Chauve, M. Methot, J. Bouchard, O. Gang, E. Kumacheva, *Biomacromolecules* **2015**, *16*, 2455.

[25]   X. Wu, R. Moon, A. Martini, *Cellulose* **2013**, *20*, 43.

[26]   Q. Wang, J. L. Mynar, M. Yoshida, E. Lee, M. Lee, K. Okuro, K. Kinbara, T. Aida, *Nature* **2010**, *463*, 339.

[27]   K. Tashiro, M. Kobayashi, H. Tadokoro, *Macromolecules* **1977**, *10*, 413.

[28]   P. Kumar, U. N. Maiti, K. E. Lee, S. O. Kim, *Carbon* **2014**, *80*, 453.

[29]   J. T. Paci, T. Belytschko, G. C. Schatz, *The Journal of Physical Chemistry C* **2007**, *111*, 18099.

[30]   J. T. Robinson, M. Zalalutdinov, J. W. Baldwin, E. S. Snow, Z. Wei, P. Sheehan, B. H. Houston, *Nano Lett* **2008**, *8*, 3441.

[31]   A. Nakayama, A. Kakugo, J. P. Gong, Y. Osada, M. Takai, T. Erata, S. Kawano, *Advanced Functional Materials* **2004**, *14*, 1124.

[32]   B. J. DeKosky, N. H. Dormer, G. C. Ingavle, C. H. Roatch, J. Lomakin, M. S. Detamore, S. H. Gehrke, *Tissue Eng Part C Methods* **2010**, *16*, 1533.

[33]   J. S. Temenoff, K. A. Athanasiou, R. G. Lebaron, A. G. Mikos, *Journal of Biomedical Materials Research* **2002**, *59*, 429.

[34]   M. B. Bryning, D. E. Milkie, M. F. Islam, L. A. Hough, J. M. Kikkawa, A. G. Yodh, *Adv Mater* **2007**, *19*, 661.

[35]   K. H. Kim, Y. Oh, M. F. Islam, *Nat Nano* **2012**, *7*, 562.